Node Feature Kernels Increase Graph Convolutional Network Robustness

Mohamed El Amine Seddik
Huawei
Paris, France
mohamed.seddik@huawei.com

Changmin Wu
Ecole Polytechnique
Palaiseau, France
changmin.wu@polytechnique.edu

Johannes F. Lutzeyer
Ecole Polytechnique
Palaiseau, France
johannes.lutzeyer@polytechnique.edu

Michalis Vazirgiannis
Ecole Polytechnique
Palaiseau, France
mvazirg@lix.polytechnique.fr

Abstract

The robustness of the much used Graph Convolutional Networks (GCNs) to perturbations of their input is becoming a topic of increasing importance. In this paper the *random* GCN is introduced for which a random matrix theory analysis is possible. This analysis suggests that if the graph is sufficiently perturbed, or in the extreme case random, then the GCN fails to benefit from the node features. It is furthermore observed that enhancing the message passing step in GCNs by adding the node feature kernel to the adjacency matrix of the graph structure solves this problem. An empirical study of a GCN utilised for node classification on six real datasets further confirms the theoretical findings and demonstrates that perturbations of the graph structure can result in GCNs performing significantly worse than Multi-Layer Perceptrons run on the node features alone. In practice, adding a node feature kernel to the message passing of perturbed graphs results in a significant improvement of the GCN's performance, thereby rendering it more robust to graph perturbations. Our code is publicly available at: https://github.com/ChangminWu/RobustGCN.

1 Introduction

In recent years Graph Neural Networks (GNNs) have been a highly impactful model type for the analysis of graph data. This is mainly due to their dominating empirical performance and ability to process attributed graphs composed of node information and an underlying graph structure. Many GNN architectures have been proposed, successively improving on weaknesses of previous architectures (e.g. Corso et al. (2020), Hamilton et al. (2017), Xu et al. (2019)). A popular GNN architecture which has remained a benchmark throughout the past years, partly due to the simplicity of its model equation and partly due to its good performance is the Graph Convolutional Network (GCN) (Kipf & Welling 2017). The GCN is part of a class of GNNs called message passing neural networks (Gilmer et al. 2017), where the computations are split into a message passing step in which node features are aggregated over neighbourhoods in the underlying graph structure and an update step in which node features are processed, most commonly by a Multi-Layer Perceptron (MLP).

While much work is being done in the empirical exploration of GNNs, in general, relatively fewer advances have been made in their theoretical analysis. A major advance in the theoretical line of research was the expressivity analysis of different message passing operators performed by Xu et al. (2019) and Morris et al. (2019). This analyses inspired many researchers to further investigate the expressivity of GNNs and resulted in a multitude of new architectures being proposed (Maron et al.

Preprint. Under review.

2019, Dasoulas et al. 2020). Another upcoming topic in the development of GNNs is their robustness to perturbations of the underlying graph structure (Zügner & Günnemann 2019, Sun et al. 2020).

In the presented work, we introduce the *random* GCN, in which parameters of the update step are randomly sampled from Gaussian distributions rather than trained as is commonly the case. The *random* GCN allows us to make use of several powerful random matrix theory tools to gain a theoretical understanding of the factors driving the inference obtained from the GCN model. Our most insightful hypothesis obtained in this way is that *the message passing step dilutes (or in the extreme case completely ignores) information present in the node features if the underlying graph structure is noisy (or in the extreme case completely random)*. In our theoretical analysis we observe that if information of the node features is introduced to the message passing operation, then this loss of information is avoided. This leads us to hypothesise that the addition of the node feature kernel to the message passing operators in GNNs could render them more robust to noise or mispecification of the underlying graph structure.

In a second part of our presented work we test the hypotheses, obtained in our study of the *random* GCN, on the state-of-the-art GCN architecture applied to six real-world benchmark datasets. This allows us to empirically verify our theoretical insight, rendering the random features approach for theoretical analysis a promising avenue for further theoretical study of GNN architectures, and the inclusion of node feature information in the message passing step a valid method to increase the robustness of GNNs.

Our main findings may be summarised as: **(i)** We contribute both a theoretical and an empirical understanding of how graph and node feature information is processed by the GCN, and **(ii)** importantly find that the preservation of node feature information is entirely dependent on an informative underlying graph structure. **(iii)** We furthermore, propose a novel GCN message passing scheme which results in more robust inference from a GCN to structural noise.

The remainder of this paper is organised as follows. In Section 2 we introduce related literature. In Section 3 we propose the *random* GCN and analyse it using tools from random matrix theory. The theoretical insight from Section 3 is then empirically verified in Section 4, where we confirm our hypotheses on the standard GCN on six benchmark datasets and observe the robust performance of the GCN when the node feature kernel matrix is added in the message passing step.

2 Related Work

There exists an extensive literature branch which studies *adversarial attack and defence strategies on graph data* in the context of GNNs summarised in Zhou et al. (2020) and Sun et al. (2020) with the former pointing out directly the need for the development of more robust GNNs. In this paper we present one approach to robustifying the performance of GNNs to graph perturbations. In this literature the focus often lies on specific attack strategies perturbing the graph structure in order to alter the inference obtained from a GNN, most commonly the GCN, and defence strategies which aim to develop methodology which is robust to these attacks. Recent advances in this literature include, Zügner & Günnemann (2019) proposing a meta learning approach to find optimal graph perturbations. Their perturbation mechanism is found to drastically decrease the global performance of GNNs to be in some cases worse than simple benchmarks such as logistic regression run on the node features only. Zügner & Günnemann (2020) propose an algorithm which certifies robustness of individual nodes for the GCN used for node classification under perturbations of the graph structure. In Jin et al. (2021) the message passing operator in the GCN is replaced by the sum of several distance based adjacency matrices with the aim of more robust GCN performance.

This paper distinguishes itself from adversarial attacks and defence literature fundamentally in that we study untargeted, random graph perturbations which arise as a result of mispecification of the data or uncertainty in the recording methods of the networks. For this kind of perturbation we are able to provide both theoretical (on a toy data example) and empirical understanding, which enables us to offer a distinction between the node feature data and the graph data in networks data sets and how these different information sources are processed by a GNN architecture.

3 Analysis of the Random GCN

In this section we present our theoretical analysis and main findings. Throughout this section $\|\cdot\|$ denotes the Euclidean (resp., spectral) norm for vectors (resp., matrices); $\|\cdot\|_F$ denotes the Frobenius norm. Specifically, we consider a *random* GCN model[1], defined as

$$\mathbf{\Phi} = \sigma(\tilde{\boldsymbol{A}}\boldsymbol{X}\boldsymbol{W}), \tag{1}$$

where $\tilde{\boldsymbol{A}} \in \mathbb{R}^{n\times n}$ denotes the normalised Adjacency operator encoding the graph structure (see (3) for its definition), $\boldsymbol{X} \in \mathbb{R}^{n\times p}$ corresponds to the node features, $\boldsymbol{W} \in \mathbb{R}^{p\times d}$ is a random matrix with $W_{ij} \sim \mathcal{N}(0,1)$ independent and identically distributed (i.i.d.) and σ is an activation function applied entry-wise. In particular, we will study the spectral behaviour of the *Gram matrix*[2] defined as

$$\boldsymbol{G} = \frac{1}{d}\mathbf{\Phi}\mathbf{\Phi}^{\intercal} = \frac{1}{d}\sigma(\tilde{\boldsymbol{A}}\boldsymbol{X}\boldsymbol{W})\sigma(\boldsymbol{W}^{\intercal}\boldsymbol{X}^{\intercal}\tilde{\boldsymbol{A}}^{\intercal}). \tag{2}$$

To analyse $\boldsymbol{G}$ we require assumptions on the node features and graph structure.

Assumption 1 (Node features)**.** *We suppose that $\boldsymbol{X}^{\intercal} = [\boldsymbol{x}_1, \ldots, \boldsymbol{x}_n] \in \mathbb{R}^{p\times n}$, where $\boldsymbol{x}_1, \ldots, \boldsymbol{x}_n$ are independent node feature vectors, each being a sample from one of $k = 2$ distribution classes $\mathcal{C}_1$ and $\mathcal{C}_2$. We further assume that the node feature vectors $\boldsymbol{x}_i$ follow a Gaussian mixture model; Specifically, for $\boldsymbol{x}_i \in \mathcal{C}_a$, $\boldsymbol{x}_i = (-1)^a \frac{\boldsymbol{\mu}}{\sqrt{p}} + \boldsymbol{z}_i$ for some vector $\boldsymbol{\mu} \in \mathbb{R}^p$ and $\boldsymbol{z}_i \sim \mathcal{N}(\mathbf{0}, \boldsymbol{I}_p/p)$.*

We stress that Assumption 1 might be relaxed to a larger class of random vectors $\boldsymbol{x} \in \mathcal{X}$, where $\mathcal{X}$ denotes any normed space, satisfying the concentration property $\mathbb{P}(|\varphi(\boldsymbol{x}) - \mathbb{E}[\varphi(\boldsymbol{x})]| > t) \leq Ce^{-(t/\sigma)^q}$ with $q \in \mathbb{R}^+$, for all 1-Lipschitz functions $\varphi : \mathcal{X} \to \mathbb{R}$. Such vectors are called *random concentrated vectors* and have the particular property to be stable by Lipschitz transformations (Louart & Couillet 2018). The simplest example of concentrated vectors is the standard Gaussian vector $\boldsymbol{z} \sim \mathcal{N}(\mathbf{0}, \boldsymbol{I}_p)$ (Ledoux 2005). A more complicated class of examples arises from the fact that the concentration property is stable through Lipschitz maps: if $\boldsymbol{z} \in \mathbb{R}^d$ is concentrated and $g : \mathbb{R}^d \to \mathbb{R}^p$ is 1-Lipschitz, then $g(\boldsymbol{z})$ is also concentrated. A large family of *generative models* falls under this more complicated class of examples, such as, the "fake" images generated by Generative Adversarial Networks due to these images being constructed as Lipschitz transformations of random Gaussian vectors (Seddik et al. 2020).

Now we introduce the underlying model that defines the graph structure. We assume that the adjacency matrix $\boldsymbol{A}$ of the graph is generated by a stochastic block model (Karrer & Newman 2011).

Assumption 2 (Graph structure)**.** *We assume that the entries of $\boldsymbol{A}$ are independent (except for $A_{ii} = 1$ for all i) Bernoulli random variables with parameter $\pi_{ij} = q^2 C_{ab} \in (0,1)$ for $\boldsymbol{x}_i \in \mathcal{C}_a$ and $\boldsymbol{x}_j \in \mathcal{C}_b$. In particular, $q \in (0,1)$ represents the probability of an edge occurring between two nodes, while C_{ab} represents the probability of an edge arising between nodes in classes $\mathcal{C}_a$ and $\mathcal{C}_b$.*

Therefore, we consider that the normalised Adjacency operator in (1) is defined as

$$\tilde{\boldsymbol{A}} = \frac{1}{\sqrt{n}}\left(\boldsymbol{A} - \boldsymbol{q}\boldsymbol{q}^{\intercal}\right), \tag{3}$$

where $\boldsymbol{q} = q\mathbf{1}_n$[3]. Note that since we make the analysis in the asymptotic regime where $n \to \infty$ (see Assumption 3 subsequently), the centring with $\boldsymbol{q}\boldsymbol{q}^{\intercal}$ and the normalisation by $\frac{1}{\sqrt{n}}$ are required so that $\tilde{\boldsymbol{A}}$ has a bounded spectral norm asymptotically.

Remark 3.1. *Assumption 2 allows us to sample directed as well as undirected graphs. Often the spectral analysis of graphs needs to be restricted to undirected graphs, since the analysis of complex-valued spectra arising for directed graphs poses a significant challenge. We are able to include directed graphs since the Gram matrix, analysed in Section 3.1, and $\tilde{\boldsymbol{X}}\tilde{\boldsymbol{X}}^{\intercal}$, analysed in Section 3.2, have real spectra even if the underlying graph structure is directed.*

[1] In Section 4.1, we show that the performance of the large *random* GCN matches that of the vanilla GCN.

[2] $\boldsymbol{G}$ provides access to the internal functioning and performance evaluation of the random GCN.

[3] The vectors $\boldsymbol{q}$ can be consistently estimated through the degree vector $\boldsymbol{d} = \boldsymbol{A}\mathbf{1}_n$ as $\boldsymbol{q} \approx \boldsymbol{d}/\sqrt{\boldsymbol{d}^{\intercal}\mathbf{1}_n}$.

3.1 Spectral Behaviour of the Gram Matrix

Let $\tilde{\boldsymbol{X}}^\intercal = [\tilde{\boldsymbol{x}}_1, \ldots, \tilde{\boldsymbol{x}}_n] = \boldsymbol{X}^\intercal \tilde{\boldsymbol{A}} \in \mathbb{R}^{p\times n}$, the entries of the Gram matrix defined in (2) are given by

$$G_{ij} = \frac{1}{d}\sigma(\boldsymbol{W}\tilde{\boldsymbol{x}}_i)^\intercal \sigma(\boldsymbol{W}\tilde{\boldsymbol{x}}_j) = \frac{1}{d}\sum_{\ell=1}^{d} \sigma(\boldsymbol{w}_\ell^\intercal \tilde{\boldsymbol{x}}_i)\sigma(\boldsymbol{w}_\ell^\intercal \tilde{\boldsymbol{x}}_j),$$

where $\boldsymbol{w}_\ell^\intercal$ denotes the ℓ-th row of $\boldsymbol{W}$. Since all the $\boldsymbol{w}_\ell$ follow the same distribution $\mathcal{N}(\boldsymbol{0}, \boldsymbol{I}_n)$, taking the expectation over $\boldsymbol{w} \sim \mathcal{N}(\boldsymbol{0}, \boldsymbol{I}_n)$ (conditionally on $\boldsymbol{X}$ and $\boldsymbol{A}$) yields the average Gram matrix $\bar{\boldsymbol{G}}$ defined with entries

$$\bar{\boldsymbol{G}}_{ij} = \bar{\boldsymbol{G}}(\tilde{\boldsymbol{x}}_i, \tilde{\boldsymbol{x}}_j) = \mathbb{E}_{\boldsymbol{w}|\boldsymbol{X},\boldsymbol{A}}\left[\sigma(\boldsymbol{w}^\intercal \tilde{\boldsymbol{x}}_i)\sigma(\boldsymbol{w}^\intercal \tilde{\boldsymbol{x}}_j)\right] \tag{4}$$

In particular, in the large n, p, d limit, it has been shown in (Louart et al. 2018) that the spectrum (and largest eigenvectors) of $\boldsymbol{G}$ are fully described by $\bar{\boldsymbol{G}}$. Specifically, the *resolvent* of $\boldsymbol{G}$ defined as,

$$\boldsymbol{Q}(z) = (\boldsymbol{G} + z\boldsymbol{I}_n)^{-1}, \tag{5}$$

for $z \in \mathbb{C}_+$ (with $\Im(z) > 0$), has a *deterministic equivalent*[4] $\bar{\boldsymbol{Q}}(z)$ (conditionally on $\boldsymbol{X}$ and $\boldsymbol{A}$). In other words, for all $\boldsymbol{M} \in \mathbb{R}^{n\times n}$ and $\boldsymbol{u}, \boldsymbol{v} \in \mathbb{R}^n$ of bounded spectral and Euclidean norms, respectively, with probability one, $\frac{1}{n}\operatorname{Tr}\left(\boldsymbol{M}(\boldsymbol{Q}(z) - \bar{\boldsymbol{Q}}(z))\right) \to 0, \quad \boldsymbol{u}^\intercal(\boldsymbol{Q}(z) - \bar{\boldsymbol{Q}}(z))\boldsymbol{v} \to 0,$ which we will simply express using the notation $\boldsymbol{Q}(z) \leftrightarrow \bar{\boldsymbol{Q}}(z)$.

A large dimensional growth rate assumption provides the existence of $\bar{\boldsymbol{Q}}(z)$.

Assumption 3 (Growth rate)**.** *As $n \to \infty$,* ***1.*** *$p/n \to c \in (0,\infty)$ and $d/n \to r \in (0,\infty)$;* ***2.*** *$\limsup_n \|\tilde{\boldsymbol{X}}\| < \infty$[5] and $|\mathcal{C}_a|/n \to c_a \in (0,1)$;* ***3.*** *$\sigma$ is λ_σ-Lipschitz continuous with $\lambda_\sigma > 0$ constant.*

Under Assumption 3, we have from (Louart et al. 2018)

$$\boldsymbol{Q}(z) \leftrightarrow \bar{\boldsymbol{Q}}(z) = \left(\frac{\bar{\boldsymbol{G}}}{1+\delta_g(z)} + z\boldsymbol{I}_n\right)^{-1}, \tag{6}$$

where $\delta_g(z)$ is the unique positive solution to the fixed point equation $\delta_g(z) = \frac{1}{n}\operatorname{Tr}(\bar{\boldsymbol{G}}\bar{\boldsymbol{Q}}(z))$.

From (6), to describe the behaviour of $\boldsymbol{G}$ one needs to address the non-linearity σ in the matrix $\bar{\boldsymbol{G}}$, this is achieved by approximating $\bar{\boldsymbol{G}}$ by a more tractable form in the large n limit. An additional regularity condition on σ is needed which we formulate in the following assumption.

Assumption 4 (Regularity of σ)**.** *Suppose that σ is twice differentiable with $\limsup_{n,x\in\mathbb{R}} |\sigma''(x)| < \infty$. Furthermore, for $\xi \sim \mathcal{N}(0,1)$ suppose $\mathbb{E}[\sigma(\xi)] = 0$ and $\mathbb{E}[\sigma^2(\xi)] = 1$.*

Denote the quantity $b_\sigma = \mathbb{E}[\sigma'(\xi)]$. Under Assumptions 3-4, from (Fan & Wang 2020, Lemma F.1), the average Gram matrix $\bar{\boldsymbol{G}}$ can be approximated by the $n \times n$ matrix $\tilde{\boldsymbol{G}} = b_\sigma^2 \tilde{\boldsymbol{X}}\tilde{\boldsymbol{X}}^\intercal + (1-b_\sigma^2)\boldsymbol{I}_n$, since almost surely as $n \to \infty$

$$\frac{1}{n}\|\bar{\boldsymbol{G}} - \tilde{\boldsymbol{G}}\|_F^2 \to 0. \tag{7}$$

This approximation ensures in particular that $\bar{\boldsymbol{G}}$ and $\tilde{\boldsymbol{G}}$ share the same spectrum.

Remark 3.2. *The approximation of $\bar{\boldsymbol{G}}$ by $\tilde{\boldsymbol{G}}$ in (7) is valid when the matrix $\tilde{\boldsymbol{X}}\tilde{\boldsymbol{X}}^\intercal$ is of bounded spectral norm. This will be ensured in Assumption 5 where additional assumptions are placed on our model parameters $\boldsymbol{\mu}$ and C_{ab}. Furthermore, since the node features $\boldsymbol{x}_i$'s form a Gaussian mixture model (as per Assumption 1), if $\tilde{\boldsymbol{A}}$ has a bounded spectral norm , then the matrix $\tilde{\boldsymbol{X}}$ falls under the setting of (Fan & Wang 2020) in which the relation in (7) holds.*

[4] Such a deterministic equivalent is a standard object within random matrix theory (Hachem et al. 2007) since it allows us to characterise the behaviour of the eigenvalues of $\boldsymbol{G}$ as well as its largest (often informative) eigenvectors. Specifically, the *spectral measure* $\mu_n = \frac{1}{n}\sum_{i=1}^n \delta_{\lambda_i(\boldsymbol{G})}$ of $\boldsymbol{G}$ (where $\lambda_i(\boldsymbol{G})$ denotes the i^{th} eigenvalue of $\boldsymbol{G}$) is related to $\boldsymbol{Q}(z)$ through the *Stieltjes transform* $q_n(z) = \int (t-z)^{-1}\mu_n(dt) = \frac{1}{n}\operatorname{Tr}(\boldsymbol{Q}(-z))$. While the eigenvector $\hat{\boldsymbol{u}}_i \in \mathbb{R}^n$ corresponding to eigenvalue $\lambda_i(\boldsymbol{G})$ is related to $\boldsymbol{Q}(z)$ through the Cauchy-integral $\hat{\boldsymbol{u}}_i\hat{\boldsymbol{u}}_i^\intercal = \frac{-1}{2\pi i}\oint_{\Gamma_i} \boldsymbol{Q}(-z)dz$ where Γ_i is a positively oriented complex contour surrounding $\lambda_i(\boldsymbol{G})$.

[5] This assumption holds if additional assumptions on the node feature mean vector $\boldsymbol{\mu}$ and the graph parameters C_{ab}, which shall be provided Assumption 5, are placed.

Since the behaviour of the average Gram matrix $\bar{\boldsymbol{G}}$ reduces to the analysis of the spectral behaviour of the matrix $\tilde{\boldsymbol{X}}\tilde{\boldsymbol{X}}^\intercal$ as per the approximation in (7), we will analyse $\tilde{\boldsymbol{X}}\tilde{\boldsymbol{X}}^\intercal$ for the remainder of Section 3.

3.2 Spectral Behaviour of $\tilde{X}\tilde{X}^\intercal$

We first need further controls on the quantities $\boldsymbol{\mu}$ and C_{ab} as we describe in the following assumption.

Assumption 5. *As $n \to \infty$, **1.** $\limsup_n \|\boldsymbol{\mu}\| < \infty$; **2.** $C_{aa} = 1 + \frac{(-1)^a \eta}{\sqrt{n}}$ for $a \in \{1,2\}$ and $C_{ab} = 1$ for $a \neq b$, where $\eta \in \mathbb{R}$ such that $\limsup_n \eta < \infty$.*

Remark 3.3. *Assumption 5.2 defines a dense graph such that the clustering with spectral methods is not asymptotically trivial. Real-World graphs are usually sparse and fall within our theoretical analysis by considering the entry-wise multiplication of the adjacency matrix $\boldsymbol{A}$ by a random binary mask as is done by Zarrouk et al. (2020).*

Our main technical result (Theorem 3.4) provides a deterministic equivalent for the resolvent of $\tilde{\boldsymbol{X}}\tilde{\boldsymbol{X}}^\intercal$ defined as

$$\boldsymbol{Q}_{\tilde{\boldsymbol{X}}}(z) = \left(\tilde{\boldsymbol{X}}\tilde{\boldsymbol{X}}^\intercal + z\boldsymbol{I}_n\right)^{-1}. \tag{8}$$

Theorem 3.4. *Define the quantities $\gamma_f = \|\boldsymbol{\mu}\|^2$, $\gamma_g = q^2\eta$, $\nu = q^2(1-q^2)$ and the matrices*

$$\boldsymbol{U} = [\bar{\boldsymbol{y}} \quad \boldsymbol{\phi}] \in \mathbb{R}^{n\times 2}, \quad \boldsymbol{B} = \begin{bmatrix} \gamma_g^2(\frac{\gamma_f}{c}+1) & \gamma_g(\frac{\gamma_f}{c}+1) \\ \gamma_g(\frac{\gamma_f}{c}+1) & \frac{\gamma_f}{c} \end{bmatrix}, \quad \boldsymbol{T} = \begin{bmatrix} 1 & 0 \\ 0 & \nu \end{bmatrix},$$

where $\bar{\boldsymbol{y}} = \frac{\boldsymbol{y}}{\sqrt{n}}$ (with $\boldsymbol{y} \in \{-1,1\}^n$ the vector of labels) and $\boldsymbol{\phi} = \frac{1}{\sqrt{n}}\boldsymbol{N}\bar{\boldsymbol{y}}$ with $\boldsymbol{N} \in \mathbb{R}^{n\times n}$ a random matrix having random i.i.d. entries with zero mean and variance ν. Under Assumptions 1, 2, 3 and 5, the resolvent $\boldsymbol{Q}_{\tilde{\boldsymbol{X}}}(z)$ has a deterministic[6] equivalent defined as

$$\bar{\boldsymbol{Q}}_{\tilde{\boldsymbol{X}}}(z) = \zeta \cdot (1+\delta_1)\left(\boldsymbol{I}_n - \zeta \boldsymbol{U}\left[\boldsymbol{B}^{-1} + \zeta\boldsymbol{T}\right]^{-1}\boldsymbol{U}^\intercal\right),$$

where $\zeta = \frac{1+\delta_2}{\nu + z(1+\delta_1)(1+\delta_2)}$ and (δ_1, δ_2) is the unique couple solution of the fixed point equations system

$$\delta_1 = \frac{1}{c}\frac{\nu(1+\delta_1)}{\nu + z(1+\delta_1)(1+\delta_2)}, \; \delta_2 = \frac{\nu(1+\delta_2)}{\nu + z(1+\delta_1)(1+\delta_2)}.$$

Sketch of proof. The proof starts by determining a random equivalent of the adjacency matrix $\boldsymbol{A}$. Since A_{ij} is Bernoulli distributed (see Assumption 2) with parameter $q^2(1 + (-1)^{k_i}\delta_{k_i=k_j}\eta/\sqrt{n})$ with $k_i \in \{1,2\}$ the class of node i, we may write $A_{ij} = q^2 + q^2(-1)^{k_i}\delta_{k_i=k_j}\eta/\sqrt{n} + N_{ij}$ where N_{ij} is a zero mean random variable with variance $\nu + \mathcal{O}(n^{-\frac{1}{2}})$. Hence, $\|\tilde{\boldsymbol{A}} - (q^2\eta\bar{\boldsymbol{y}}\bar{\boldsymbol{y}}^\intercal + \frac{1}{\sqrt{n}}\boldsymbol{N})\| \to 0$ as $n \to \infty$. Finally, exploiting standard random matrix theory tools from (Hachem et al. 2007, Louart & Couillet 2018) provides the deterministic equivalent $\bar{\boldsymbol{Q}}_{\tilde{\boldsymbol{X}}}(z)$. □

In essence, Theorem 3.4 shows that the deterministic equivalent $\bar{\boldsymbol{Q}}_{\tilde{\boldsymbol{X}}}(z)$ is composed of two main terms: a diagonal matrix $\zeta \cdot (1+\delta_1)\boldsymbol{I}_n$, which describes the behaviour of the noise in the data model (both adjacency and node features), and an informative rank-2 matrix $\boldsymbol{U}\left[\boldsymbol{B}^{-1} + \zeta\boldsymbol{T}\right]^{-1}\boldsymbol{U}^\intercal$ which correlates with the vector of labels $\bar{\boldsymbol{y}}$ if the adjacency matrix and/or the node features are informative, i.e., values γ_g and γ_f, respectively, are sufficiently large. Figure 1(a) and (b) depict a histogram of the eigenvalues of $\tilde{\boldsymbol{X}}\tilde{\boldsymbol{X}}^\intercal$ which converges to the limiting distribution described by Theorem 3.4, as well as its dominant eigenvector which correlates with $\bar{\boldsymbol{y}}$. Importantly, our analysis allows us to conclude that when the graph structure is completely noisy (i.e., $\eta = 0$), the dominant eigenvector of $\tilde{\boldsymbol{X}}\tilde{\boldsymbol{X}}^\intercal$ is no longer aligned with $\bar{\boldsymbol{y}}$ even if the node features are informative (i.e., γ_f large) as will be more clearly visible in Corollary 3.5.

[6]The matrix $\bar{\boldsymbol{Q}}_{\tilde{\boldsymbol{X}}}(z)$ is not deterministic since it depends on the random vector $\boldsymbol{\phi}$. However, since we are interested in evaluating quantities of the forms $\frac{1}{n}\operatorname{Tr}(\boldsymbol{M}\bar{\boldsymbol{Q}}_{\tilde{\boldsymbol{X}}}(z))$ or $\boldsymbol{u}^\intercal\bar{\boldsymbol{Q}}_{\tilde{\boldsymbol{X}}}(z)\boldsymbol{v}$ for $\boldsymbol{M}$, $\boldsymbol{u}$ and $\boldsymbol{v}$ independent of $\boldsymbol{\phi}$, $\bar{\boldsymbol{Q}}_{\tilde{\boldsymbol{X}}}(z)$ has a deterministic behaviour asymptotically as $n \to \infty$.

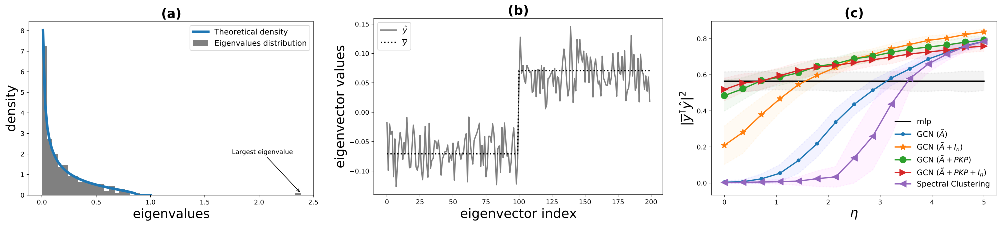

Figure 1: **(a)** Eigenvalues distribution of $\tilde{\boldsymbol{X}}\tilde{\boldsymbol{X}}^\intercal$ versus the theoretical density as per Theorem 3.4 (the theoretical density is obtained as $f(x) = \frac{1}{\pi}\lim_{\epsilon\to 0}\Im[q(x+i\epsilon)]$ where $q(z) = \frac{1}{n}\operatorname{Tr}(\bar{\boldsymbol{Q}}_{\tilde{\boldsymbol{X}}}(z))$). **(b)** Eigenvector of $\tilde{\boldsymbol{X}}\tilde{\boldsymbol{X}}^\intercal$ corresponding to its largest eigenvalue which correlates with $\bar{\boldsymbol{y}}$. The parameters are: $p = 1000$, $n = 200$, $q = 0.5$, $\eta = 4$ and $\boldsymbol{\mu} = [2, \boldsymbol{0}_{p-1}]^\intercal$. **(c)** Alignment between the largest eigenvector of $\tilde{\boldsymbol{X}}\tilde{\boldsymbol{X}}^\intercal$ and the labels vector $\bar{\boldsymbol{y}}$ for different added node feature kernel message passing strategies in terms of η. The different parameters are: $p = 500$, $n = 250$, $q = 0.4$, $\boldsymbol{\mu} = [1.7, \boldsymbol{0}_{p-1}]^\intercal$ and the kernel matrix has entries $K_{ij} = \boldsymbol{x}_i^\intercal \boldsymbol{x}_j$, mean and std computed over 100 runs. ***The GCN with message passing operator $\tilde{A} + \boldsymbol{PKP}$ outperforms other models when the graph structure is noisy (i.e., low values of η).***

Corollary 3.5 (Case $\eta = 0$)**.** *Recall the notation and Assumptions of Theorem 3.4, for $\eta = 0$ (i.e., a non-informative graph structure), $\bar{\boldsymbol{Q}}_{\tilde{\boldsymbol{X}}}(z)$ takes the form*

$$\bar{\boldsymbol{Q}}_{\tilde{\boldsymbol{X}}}(z) = \zeta \cdot (1+\delta_1)\left(\boldsymbol{I}_n - \frac{\zeta^2\gamma_f}{c+\zeta\nu\gamma_f}\boldsymbol{\phi}\boldsymbol{\phi}^\intercal\right). \tag{9}$$

And, for $\hat{\boldsymbol{y}}$ the eigenvector of $\tilde{\boldsymbol{X}}\tilde{\boldsymbol{X}}^\intercal$ corresponding to its largest eigenvalue, $|\bar{\boldsymbol{y}}^\intercal\hat{\boldsymbol{y}}|^2 \to_{n\to\infty} 0$.

Sketch of proof. Expression (9) follows from Theorem 3.4 by simply taking the limit as $\eta \to 0$. The second part of the Corollary is obtained by computing $|\bar{\boldsymbol{y}}^\intercal\hat{\boldsymbol{y}}|^2 = \frac{-1}{2i\pi}\oint_\Gamma \bar{\boldsymbol{y}}^\intercal \boldsymbol{Q}_{\tilde{\boldsymbol{X}}}(-z)\bar{\boldsymbol{y}}dz$ where Γ is a small positively oriented complex contour surrounding the largest eigenvalue of $\tilde{\boldsymbol{X}}\tilde{\boldsymbol{X}}^\intercal$. Hence, using $\bar{\boldsymbol{Q}}_{\tilde{\boldsymbol{X}}}(z)$ as a proxy allows us to state $|\bar{\boldsymbol{y}}^\intercal\hat{\boldsymbol{y}}|^2 + \frac{1}{2i\pi}\oint_\Gamma \bar{\boldsymbol{y}}^\intercal\bar{\boldsymbol{Q}}_{\tilde{\boldsymbol{X}}}(-z)\bar{\boldsymbol{y}}dz \to 0$ almost surely as $n\to\infty$. The final result is obtained by showing that $\bar{\boldsymbol{y}}^\intercal\boldsymbol{\phi}\boldsymbol{\phi}^\intercal\bar{\boldsymbol{y}}$ concentrates around its expectation with $\mathbb{E}[\bar{\boldsymbol{y}}^\intercal\boldsymbol{\phi}\boldsymbol{\phi}^\intercal\bar{\boldsymbol{y}}] = \frac{1}{n}\operatorname{Var}[\bar{\boldsymbol{y}}^\intercal\boldsymbol{N}\bar{\boldsymbol{y}}] = \frac{\nu}{n} \to 0$ and by evaluating $\frac{1}{2i\pi}\oint_\Gamma \zeta(-z)(1+\delta_1(-z))dz = 0$. $\square$

The main conclusion from Corollary 3.5 is that when the graph structure is completely random (when $\eta = 0$, $\|\tilde{\boldsymbol{A}} - \frac{1}{\sqrt{n}}\boldsymbol{N}\| \to 0$), the largest eigenvector of $\tilde{\boldsymbol{X}}\tilde{\boldsymbol{X}}^\intercal$ (which is intuitively supposed to be informative) does not correlate with the labels vector $\bar{\boldsymbol{y}}$ independently of the information contained in the node features. To overcome this issue, a standard solution (which already exists in the GCN literature) is to use self-loops by using the matrix $\tilde{\boldsymbol{A}} + \boldsymbol{I}_n$ instead of $\tilde{\boldsymbol{A}}$[7]. However, using only self-loops is insufficient to make the message passing informative and hence we propose in Section 3.3 to utilise node feature kernels to ensure the preservation of node feature information.

3.3 Message Passing through Node Feature Kernels

As we discussed in Section 3.2, when the graph structure (in the extreme case) is completely random, the *random* GCN model fails to extract information from the node features. To make the message passing informative and thereby to robustify the GCN, we propose to consider the operator $\tilde{\boldsymbol{A}} + \bar{\boldsymbol{K}}$ instead of $\tilde{\boldsymbol{A}}$, where $\bar{\boldsymbol{K}}$ is a kernel matrix computed on the node features $\boldsymbol{X}$. Indeed, let $\boldsymbol{K}$ be a matrix with entries $K_{ij} = \kappa(\boldsymbol{x}_i^\intercal\boldsymbol{x}_j)$ for some smooth function $\kappa : \mathbb{R}\to\mathbb{R}$. Relying on (El Karoui et al. 2010), the kernel matrix $\boldsymbol{K}$ can be approximated in spectral norm asymptotically as $n\to\infty$ by

$$\tilde{\boldsymbol{K}} = \kappa(0)\boldsymbol{1}_n\boldsymbol{1}_n^\intercal + \kappa'(0)\left(\frac{\gamma_f}{c}\bar{\boldsymbol{y}}\bar{\boldsymbol{y}}^\intercal + \boldsymbol{Z}\boldsymbol{Z}^\intercal\right) + \boldsymbol{\Delta}, \tag{10}$$

where $\boldsymbol{\Delta} = \frac{\kappa''(0)}{2p}\boldsymbol{1}_n\boldsymbol{1}_n^\intercal + (\kappa(1) - \kappa(0) - \frac{\gamma_f}{c}\kappa'(0))\boldsymbol{I}_n$. Hence, considering the matrix $\tilde{\boldsymbol{A}} + \boldsymbol{PKP}$, where $\boldsymbol{P} = \boldsymbol{I}_n - \frac{1}{n}\boldsymbol{1}_n\boldsymbol{1}_n^\intercal$ (the centring matrix), maintains the informative nature of the message

[7]Note that $A_{ii} = 1$ for all i from Assumption 2, but this is equivalent to assuming $A_{ii} = 0$ for all i since the normalisation by $\sqrt{n}$ in (3) makes $\frac{1}{\sqrt{n}}\boldsymbol{I}_n$ of vanishing spectral norm asymptotically.

passing step (through the term $\frac{\gamma_f}{c}\bar{\boldsymbol{y}}\bar{\boldsymbol{y}}^\intercal$) even in the case where the operator $\tilde{\boldsymbol{A}}$ is not informative. Intuitively, the addition of the node feature kernel can be interpreted as considering both the originally recorded graph and a node feature similarity graph in the message passing architecture. This addition gives GNNs the necessary expressive ability to preserve information present in the node features, which is lost in the case of uninformative or noisy graph structures.

Figure 1(c) shows the performance of different message passing strategies (compared to random MLP and spectral clustering; involving only node features or adjacency matrix respectively) which confirms the effectiveness of introducing node feature kernel in the regime where the graph similarity is noisy (i.e., low values of η), a property which is also confirmed to be valid for practical GCNs as we will discuss in Section 4.

4 Experiments

In order to validate our theoretical findings in real-world scenarios, we experiment on the node classification task using GCNs on perturbed data. In Section 4.1, we begin by justifying the use of the *random* GCN in the theoretical analysis, and then discuss results from two sets of experiments: firstly, we directly apply our theoretical model to real datasets and observe results consistent with the theoretical analysis secondly, we propose a realistic perturbation scheme on the edges and demonstrate that explicitly adding extra information from the node features (via their kernel) helps to robustify the performance of GCNs to this perturbation. Finally, we show that the observed phenomena extend to deeper GCN architectures and cases with node feature perturbations.

We work with six node classification benchmark datasets, which are the three well-studied citation networks of Cora, CiteSeer and PubMed (Sen et al. 2008), an extended version of Cora (Bojchevski & Günnemann 2018), called CoraFull, and two Amazon co-purchase graphs of Photo and Computers (Shchur et al. 2018). In all experiments, a MLP model, which only takes the node features as input, serves as a baseline. We follow the semi-supervised node classification setting proposed by Yang et al. (2016), i.e., we use their train/valid/test split for Cora/CiteSeer/PubMed, and we randomly sample 20 nodes from each class as training set, 500 nodes as validation set and another 1000 nodes as test set for CoraFull/Photo/Computers. Each experiment is repeated 10 times. Implementation details and a summary of dataset statistics can be found in the Appendix D.

Theoretical Noise Scheme In line with the theoretical analysis, we model the noise as a separate term from the original graph,

$$\boldsymbol{X}^{(i+1)} = \sigma\left((\alpha\bar{\boldsymbol{A}} + (1-\alpha)(\boldsymbol{R} + \boldsymbol{I}_n))\boldsymbol{X}^{(i)}\boldsymbol{W}\right), \tag{11}$$

where $\bar{\boldsymbol{A}}$ is the normalised adjacency matrix commonly used in GCN, $\boldsymbol{R}$ is the noise modelled by a random Erdős-Renyi graph, $\boldsymbol{X}$ is the node embedding and the coefficient α controls the influence of the noise by weighting original graph propagation. We also define perturbation ratio, a second factor that controls the noise, as the density of noise matrix $\boldsymbol{R}$ divided by the density of original graph. Since the noise and original graph have the same number of nodes, the perturbation ratio equals the ratio between their number of edges, denoted by $|E_{\boldsymbol{R}}|$ and $|E|$.

Realistic Noise Scheme We consider two more realistic noise schemes, where only the perturbed graph $\hat{\mathcal{G}}(\boldsymbol{X}, \hat{\boldsymbol{A}}, \hat{E})$ is known to us. In the first scheme which we refer to as *edge deletion*, a certain amount of existing edges are randomly sampled and removed from original graph, rendering the perturbed graph a subgraph of the unperturbed graph; while in the second scheme, which we refer to as *edge insertion*, we add to the original graph a certain amount of connections sampled from its non-existing edges. We vary the number of edges removed/added and observe the model performance change with respect to the edge change ratio or the perturbation ratio, defined as the number of edges in the perturbed graph, denoted $|\hat{E}|$, vs. the number of edges in the original graph, denoted $|E|$. A node feature kernel matrix is added to study its impact in practice, as shown in the following equation,

$$\boldsymbol{X}^{(i+1)} = \sigma\left((\beta\hat{\boldsymbol{A}} + (1-\beta)\mathcal{N}(\boldsymbol{K}))\boldsymbol{X}^{(i)}\boldsymbol{W}\right), \tag{12}$$

where $\hat{\boldsymbol{A}}$ is the GCN message passing operator of the perturbed graph, $\mathcal{N}(\boldsymbol{K}) = \boldsymbol{D}_{\boldsymbol{K}}^{-1/2}\boldsymbol{K}\boldsymbol{D}_{\boldsymbol{K}}^{-1/2}$ is the normalised kernel matrix built from node features ($\boldsymbol{D}_{\boldsymbol{K}} = \mathrm{diag}(\boldsymbol{K}\boldsymbol{1}_n)$). We are degree normalising the kernel to match the graph representation of the GCN message passing operator.

Node Feature Kernels As stated in Section 3.3, we use the kernel to introduce information from the node features to the message passing structure. The choices of qualified smooth kernel functions are many. In our experiment, we perform a proof of concept using the simple linear kernel, defined as the inner product between node features $K_{ij} = \boldsymbol{x}_i^\intercal \boldsymbol{x}_j$.

Kernel Sparsification Using the full kernel matrix, where the kernel value is recorded between every pair of nodes, is both computationally costly and may bring in redundant information. We adopt in practice a sparsification method using the adjacency matrix of the observed graph, with which (12) can be rewritten as,

$$\boldsymbol{X}^{(i+1)} = \sigma\left((\beta\hat{\boldsymbol{A}} + (1-\beta)\mathcal{N}(\boldsymbol{K} \circ \hat{\boldsymbol{A}}))\boldsymbol{X}^{(i)}\boldsymbol{W}\right), \tag{13}$$

where $\circ$ denotes Hadamard product. A consequence of this sparsification method is that the added computational cost stemming from the consideration of the node feature kernel is linear in the number of edges in the graph $|E|$ and the node feature dimension p, i.e., of order $\mathcal{O}(|E|p)$.

4.1 Experiment Analysis

Asymptotic Analysis of Random GCN To validate the practical applicability of the theoretical analysis in Section 3, we study the asymptotic behaviour of the *random* GCN, the vanilla GCN and a MLP baseline when the hidden dimension of node features grows. In Figure 2 **(top row)** we observe that with increasing hidden dimension, the performance of both the vanilla GCN and MLP remains stable, while the performance of *random* GCN converges to vanilla GCN's accuracy. Between hidden dimensions of 2000 and 3000 the performance of *random* GCN starts to match that of vanilla GCN. Hence, we have given an empirical indication of the conditions under which our theoretical model, the *random* GCN, and the vanilla GCN are equivalent.

Theoretical Noise Scheme In Figure 2 (**middle row**), we report the results of theoretical noise models, where the density of the noise is 0.1, 1 and 10 times that of the original graph, as well as the results from the aforementioned MLP baseline which is agnostic to the graph structure. Consistent with the theoretical analysis, we observe that when the graph structure information is completely destroyed (i.e., $\alpha = 0$), information from the node features is almost entirely lost, dropping drastically below the MLP, particularly in the dense noise setting. But on Photo and Computers, we observe the drop even when noise is relatively sparse (with ratio 0.1). As expected, the model performance drops quickly with decreasing weight α on the original graph propagation, when the noise is of the same or larger density as the original graph. On Photo and Computers, random noise has a greater impact as the performance drops even with a small perturbation ratio while on the others, the performance decay becomes much slower when the noise is sparser than the original graph.

Realistic Noise Scheme In this set of experiments, we study the change of model performance when the graph structure is perturbed, e.g. edges are randomly removed or added. Figure 2 (**bottom row**) shows the results over different perturbation rates and coefficients of perturbed graph propagation. The vertical line at a rate of 1 represents the performance on the unperturbed graph. On its left is the *edge deletion* case, with rate less than 1, where the most perturbed case corresponds to rate 0; on the right is the *edge insertion* case, where the perturbations grow with the rate.

Naturally the performance decreases gradually when edges are removed or added, as shown by the yellow line with coefficient β equals to 1, i.e., no kernel is added. Adding the node feature kernel (when β is smaller that 1), has a positive impact on the model performance, especially for *edge insertion* noise. The performance decreases much slower than the case without kernel, which is less observable on Photo/Computers with largely overlapped curves (area of variance) but we still have the curve $\beta = 0$ (with kernel) always above $\beta = 1$ (without kernel) on *edge insertion* case with dense noise. For *edge deletion* noise, the addition of the kernel seems to have almost no impact. This finding is consistent with the empirical results in Zügner & Günnemann (2019), where the authors find that adding edges, rather than removing them, appears more often in effective adversarial attacks on graphs. A possible explanation, inspired by our theoretical analysis, is that *the message passing step relies on community structure to be present in the graph*. Destroying community structure of the graph will not only destroy the graph structure information but also dilute the information from node features, thus causing a performance drop. Adding edges may be a more efficient way than removing edges in terms of destroying community structure.

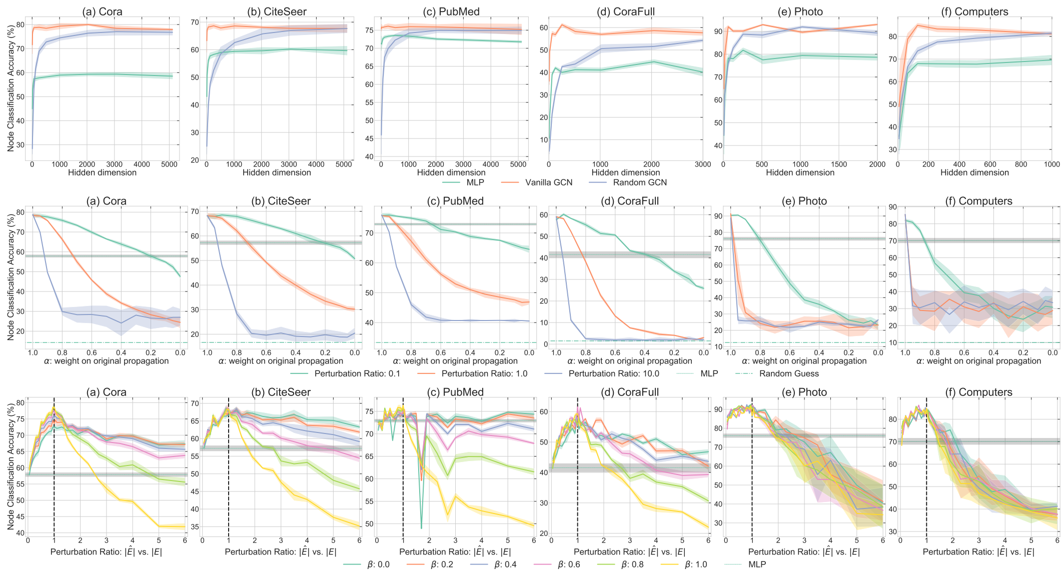

Figure 2: **(top row)** Performance change over the embedding dimension with different models: *random* GCN, vanilla GCN and MLP. **(middle row)** Performance change over the coefficient of original graph propagation, α, with different perturbation ratios. **(bottom row)** Performance change over the perturbation ratio under realistic setting with different coefficients, β, put on the noisy graph propagation.

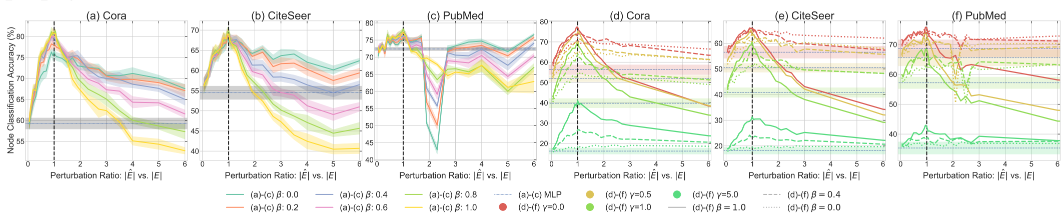

Figure 3: Experiment results for two-layer GCNs (a)-(c) and node feature noise (d)-(f).

Deeper architecture The previous experiments are based on a single-layer GCN model. In practice, the best-performing GCN models on these datasets often contain several message-passing layers and therefore, we want to observe whether our theoretical results can be extrapolated to the multi-layer case. We add an extra GCN layer to the original model and repeat our experiments on the citation network datasets. The results are shown in Figure 3 (a)-(c). Results of the remaining three datasets can be found in the Appendix F. There is no fundamental change in the observed trends and we can draw the same conclusion as we drew on the single-layer model. Additionally, we observe that the multi-layer model shows larger variation when adding noise, which could be caused by the variances that are amplified by the stacked message-passing layers.

Node feature noise We now study how node feature noise interacts with our proposed model. We perform the same experiments as in the realistic noise setting on the three citation network datasets. But add Gaussian noise $\mathcal{N}(\mathbf{0}, \gamma \operatorname{diag}(\sigma_i))$ to the node features where σ_i is the estimated variance of the i-th feature and γ is a scaling parameter. The results are recorded in Figure 3 (d)-(f). We observe that when the node feature noise is five times larger than the graph structure noise, the addition of the node feature kernel decreases the model performance as we can see from the green curves, with-kernel (dashed or dotted line) performs worse than without-kernel (solid line). However, when $\gamma \leq 1$ the performance of our kernel is robust as the observed trend matches that in Figure 2.

5 Conclusion

We have introduced, for the first time to the best of our knowledge, the *random* GCN, which we analysed theoretically using random matrix theory. Our analysis shed light on the way in which the GCN processes the different sources of information present in attributed graphs. In particular, this leads us to conclude that *perturbations of the graph structure strongly influence the performance of the GCN regardless of the information contained in the node features.* In particular, for stochastic blockmmodel graphs the presence of community structure (and the degree to which this structure is present) is required (beneficial) for a message passing scheme which leads to eigenvectors of the message passing operator's Gram matrix that align with the node labels. These conclusions were confirmed in multiple experiments with the standard GCN architecture on real-world datasets. As expected from our theoretical analysis, we empirically observed graph structure perturbations to have a strong negative impact on the performance of standard GNN architectures, which drops rapidly below the performance of a MLP using only node features. On real world data we observe the introduction of a node feature kernel to the GCN's message passing scheme to significantly improve the performance of the GCN in the presence of a noisy graph structure.We believe that the introduced random GCN model is likely to be a suitable analysis framework for further GNN models, which combined with random matrix theory can allow us to gain further insight into the inference obtained from these models.

References

Bojchevski, A. & Günnemann, S. (2018), Deep gaussian embedding of graphs: Unsupervised inductive learning via ranking, *in* '6th International Conference on Learning Representations (ICLR)', pp. 1–13.

Corso, G., Cavalleri, L., Beaini, D., Liò, P. & Veličković, P. (2020), 'Principal neighbourhood aggregation for graph nets', *arXiv:2004.05718* .

Dasoulas, G., Dos Santos, L., Scaman, K. & Virmaux, A. (2020), Coloring graph neural networks for node disambiguation, *in* 'Proceedings of the Twenty-Ninth International Joint Conference on Artificial Intelligence (IJCAI)', pp. 2126–2132.

El Karoui, N. et al. (2010), 'The spectrum of kernel random matrices', *Annals of statistics* pp. 1–50.

Fan, Z. & Wang, Z. (2020), 'Spectra of the conjugate kernel and neural tangent kernel for linear-width neural networks', *arXiv:2005.11879* .

Fey, M. & Lenssen, J. E. (2019), Fast graph representation learning with PyTorch Geometric, *in* 'ICLR Workshop on Representation Learning on Graphs and Manifolds'.

Gilmer, J., Schoenholz, S. S., Riley, P. F., Vinyals, O. & Dahl, G. E. (2017), Neural message passing for quantum chemistry, *in* 'Proceedings of the 34th International Conference on Machine Learning (ICML)', pp. 1263 – 1272.

Hachem, W., Loubaton, P., Najim, J. et al. (2007), 'Deterministic equivalents for certain functionals of large random matrices', *The Annals of Applied Probability* pp. 875–930.

Hamilton, W. L., Ying, R. & Leskovec, J. (2017), Inductive representation learning on large graphs, *in* 'Proceedings of the 31st International Conference on Neural Information Processing Systems (NIPS)', Curran Associates Inc., pp. 1025 – 1035.

Jin, M., Chang, H., Zhu, W. & Sojoudi, S. (2021), Power up! robust graph convolutional network via graph powering, *in* 'AAAI Conference on Artificial Intelligence (AAAI)'.

Karrer, B. & Newman, M. E. (2011), 'Stochastic blockmodels and community structure in networks', *Physical review E* p. 016107.

Kingma, D. P. & Ba, J. (2014), 'Adam: A method for stochastic optimization', *arXiv preprint arXiv:1412.6980* .

Kipf, T. N. & Welling, M. (2017), Semi-supervised classification with graph convolutional networks, *in* '5th International Conference on Learning Representations (ICLR)'.

Ledoux, M. (2005), *The concentration of measure phenomenon*, number 89, American Mathematical Soc.

Louart, C. & Couillet, R. (2018), 'Concentration of measure and large random matrices with an application to sample covariance matrices', *arXiv:1805.08295* .

Louart, C., Liao, Z., Couillet, R. et al. (2018), 'A random matrix approach to neural networks', *The Annals of Applied Probability* pp. 1190–1248.

Maron, H., Ben-Hamu, H., Serviansky, H. & Lipman, Y. (2019), Provably powerful graph networks, *in* 'Advances in Neural Information Processing Systems (NeurIPS)', pp. 2156 – 2167.

Morris, C., Ritzert, M., Fey, M., Hamilton, W. L., Lenssen, J. E., Rattan, G. & Grohe, M. (2019), Weisfeiler and leman go neural: Higher-order graph neural networks, *in* 'Proceedings of the AAAI Conference on Artificial Intelligence', pp. 4602 – 4609.

Seddik, M. E. A., Louart, C., Tamaazousti, M. & Couillet, R. (2020), Random matrix theory proves that deep learning representations of GAN-data behave as Gaussian mixtures, *in* 'Proceedings of the 37th International Conference on Machine Learning (ICML)', PMLR, pp. 8573–8582.

Sen, P., Namata, G., Bilgic, M., Getoor, L., Galligher, B. & Eliassi-Rad, T. (2008), 'Collective classification in network data', *AI Magazine* p. 93.

Shchur, O., Mumme, M., Bojchevski, A. & Günnemann, S. (2018), 'Pitfalls of graph neural network evaluation', *arXiv preprint arXiv:1811.05868* .

Silverstein, J. W. & Bai, Z. (1995), 'On the empirical distribution of eigenvalues of a class of large dimensional random matrices', *Journal of Multivariate analysis* **54**(2), 175–192.

Sun, L., Dou, Y., Yang, C., Wang, J., Yu, P. S. & Li, B. (2020), 'Adversarial attack and defense on graph data: A survey', *arXiv:1812.10528* .

Xu, K., Hu, W., Leskovec, J. & Jegelka, S. (2019), How powerful are graph neural networks?, *in* '7th International Conference on Learning Representations (ICLR)'.

Yang, Z., Cohen, W. & Salakhudinov, R. (2016), Revisiting semi-supervised learning with graph embeddings, *in* 'Proceedings of The 33rd International Conference on Machine Learning (ICML)', PMLR, pp. 40–48.

Zarrouk, T., Couillet, R., Chatelain, F. & Le Bihan, N. (2020), Performance-complexity trade-off in large dimensional statistics, *in* '2020 IEEE 30th International Workshop on Machine Learning for Signal Processing (MLSP)', IEEE, pp. 1–6.

Zhou, Y., Zheng, H. & Huang, X. (2020), 'Graph neural networks: Taxonomy, advances and trends', *arXiv:2012.08752* .

Zügner, D. & Günnemann, S. (2019), Adversarial attacks on graph neural networks via meta learning, *in* '7th International Conference on Machine Learning (ICLR)'.

Zügner, D. & Günnemann, S. (2020), Certifiable robustness of graph convolutional networks under structure perturbations, *in* 'Proceedings of the 26th ACM SIGKDD International Conference on Knowledge Discovery & Data Mining', pp. 1656–1665.

We provide in the appendix the necessary random matrix theory results, detailed proofs of our main results and further details on our experimentation setup and results.

A Random matrix theory background

We begin recalling several random matrix theory tools that are needed to establish our main results. First, we recall a fundamental result (Theorem A.1) from Louart & Couillet (2018) which provides a deterministic equivalent for the *resolvent* of a *sample covariance* matrix.

Theorem A.1 (Deterministic equivalent for sample covariance matrices Louart & Couillet (2018))**.** *Let $\boldsymbol{M} \in \mathbb{R}^{n\times n}$ such that $\|\boldsymbol{M}\boldsymbol{M}^\intercal\| < \infty$[8] w.r.t. n and $\tilde{\boldsymbol{Z}} \in \mathbb{R}^{n\times p}$ some random matrix with i.i.d. entries having zero mean, unit variance and a finite forth order moment. In the limit $n \to \infty$ with $p/n \to c \in (0, \infty)$, the resolvent $\boldsymbol{Q}(z) = \left(\frac{1}{p}\boldsymbol{M}\tilde{\boldsymbol{Z}}\tilde{\boldsymbol{Z}}^\intercal\boldsymbol{M}^\intercal + z\boldsymbol{I}_n\right)^{-1}$ for $z \in \mathbb{C}$ with $\Im(z) > 0$, admits a deterministic equivalent $\bar{\boldsymbol{Q}}(z)$ defined as*

$$\bar{\boldsymbol{Q}}(z) = \left(\frac{\boldsymbol{M}\boldsymbol{M}^\intercal}{1+\delta(z)} + z\boldsymbol{I}_n\right)^{-1},$$

where $\delta(z)$ is the unique solution to the fixed point equation $\delta(z) = \frac{1}{p}\operatorname{Tr}\left(\boldsymbol{M}^\intercal\bar{\boldsymbol{Q}}(z)\boldsymbol{M}\right)$.

Proof. Denote $\boldsymbol{a}_i = \boldsymbol{M}\tilde{\boldsymbol{z}}_i$, hence

$$\boldsymbol{Q}(z) = \left(\frac{1}{p}\sum_{i=1}^n \boldsymbol{a}_i\boldsymbol{a}_i^\intercal + z\boldsymbol{I}_n\right)^{-1} = \boldsymbol{Q}_{-i} - \frac{\boldsymbol{Q}_{-i}\frac{1}{p}\boldsymbol{a}_i\boldsymbol{a}_i^\intercal\boldsymbol{Q}_{-i}}{1+\frac{1}{p}\boldsymbol{a}_i^\intercal\boldsymbol{Q}_{-i}\boldsymbol{a}_i},$$

where $\boldsymbol{Q}_{-i} = \left(\frac{1}{p}\sum_{j\neq i}^n \boldsymbol{a}_j\boldsymbol{a}_j^\intercal + z\boldsymbol{I}_n\right)^{-1}$, and we also have

$$\boldsymbol{Q}(z)\boldsymbol{a}_i = \frac{\boldsymbol{Q}_{-i}\boldsymbol{a}_i}{1+\frac{1}{p}\boldsymbol{a}_i^\intercal\boldsymbol{Q}_{-i}\boldsymbol{a}_i}.$$

A deterministic equivalent for $\boldsymbol{Q}(z)$ (which approximates $\mathbb{E}[\boldsymbol{Q}(z)]$) is of the form $\bar{\boldsymbol{Q}}(z) = (\boldsymbol{F} + z\boldsymbol{I}_n)^{-1}$ for some deterministic matrix $\boldsymbol{F}$, by computing the difference $\bar{\boldsymbol{Q}}(z) - \mathbb{E}[\boldsymbol{Q}(z)]$ using the above identities, we obtain

$$\begin{aligned}\bar{\boldsymbol{Q}}(z) - \mathbb{E}[\boldsymbol{Q}(z)] &= \frac{1}{n}\sum_{i=1}^n \mathbb{E}\left[\boldsymbol{Q}_{-i}\left(\frac{\boldsymbol{a}_i\boldsymbol{a}_i^\intercal}{1+\frac{1}{p}\boldsymbol{a}_i^\intercal\boldsymbol{Q}_{-i}\boldsymbol{a}_i} - \boldsymbol{F}\right)\bar{\boldsymbol{Q}}(z)\right] \\ &+ \frac{1}{n^2}\sum_{i=1}^n \mathbb{E}\left[\boldsymbol{Q}_{-i}(z)\boldsymbol{a}_i\boldsymbol{a}_i^\intercal\boldsymbol{Q}_{-i}(z)\boldsymbol{F}\bar{\boldsymbol{Q}}(z)\right].\end{aligned}$$

It can be shown that the matrix $\frac{1}{n^2}\sum_{i=1}^n \mathbb{E}\left[\boldsymbol{Q}_{-i}(z)\boldsymbol{a}_i\boldsymbol{a}_i^\intercal\boldsymbol{Q}_{-i}(z)\boldsymbol{F}\bar{\boldsymbol{Q}}(z)\right]$ has a vanishing operator norm as $n \to \infty$. Therefore, $\boldsymbol{F}$ can be taken as

$$\boldsymbol{F} = \frac{\mathbb{E}\left[\boldsymbol{a}_i\boldsymbol{a}_i^\intercal\right]}{1+\mathbb{E}\left[\frac{1}{p}\boldsymbol{a}_i^\intercal\boldsymbol{Q}_{-i}\boldsymbol{a}_i\right]} = \frac{\boldsymbol{M}\boldsymbol{M}^\intercal}{1+\frac{1}{p}\operatorname{Tr}(\boldsymbol{M}^\intercal\mathbb{E}\left[\boldsymbol{Q}_{-i}\right]\boldsymbol{M})}$$

Which provides the defined deterministic equivalent in Theorem A.1. □

Another useful result which is known as the perturbation lemma (Silverstein & Bai 1995) is also needed here.

Lemma A.2 (Perturbation lemma Silverstein & Bai (1995))**.** *Let $\boldsymbol{A}, \boldsymbol{B} \in \mathbb{R}^{n\times n}$ some symmetric matrices, $\boldsymbol{u} \in \mathbb{R}^n$, $\gamma \in \mathbb{R}$ and $z \in \mathbb{C}$ with $\Im(z) > 0$, then*

$$\left|\operatorname{Tr}\left(\boldsymbol{A}(\boldsymbol{B}+\gamma\boldsymbol{u}\boldsymbol{u}^\intercal + z\boldsymbol{I}_n)^{-1}\right) - \operatorname{Tr}\left(\boldsymbol{A}(\boldsymbol{B}+z\boldsymbol{I}_n)^{-1}\right)\right| \leq \frac{\|\boldsymbol{A}\|}{|\Im(z)|}.$$

In particular, for $\boldsymbol{A} = \frac{1}{n}\boldsymbol{I}_n$, we have $\frac{1}{n}\operatorname{Tr}(\boldsymbol{B}+\gamma\boldsymbol{u}\boldsymbol{u}^\intercal + z\boldsymbol{I}_n)^{-1} = \frac{1}{n}\operatorname{Tr}(\boldsymbol{B}+z\boldsymbol{I}_n)^{-1} + \mathcal{O}(n^{-1})$, which shows that the spectral measure of $\boldsymbol{B}+\gamma\boldsymbol{u}\boldsymbol{u}^\intercal$ is asymptotically close to that of $\boldsymbol{B}$ in the large n limit.

[8] $\|\boldsymbol{M}\boldsymbol{M}^\intercal\|$ remains constant as n goes to infinity.

Finally, we will need the Woodbury matrix identity from the following Lemma.

Lemma A.3 (Woodbury identity)**.** *Let $\boldsymbol{A} \in \mathbb{R}^{n\times n}$ and $\boldsymbol{B} \in \mathbb{R}^{k\times k}$ invertible and $\boldsymbol{U} \in \mathbb{R}^{n\times k}$, then*

$$(\boldsymbol{A} + \boldsymbol{U}\boldsymbol{B}\boldsymbol{U}^\intercal)^{-1} = \boldsymbol{A}^{-1} - \boldsymbol{A}^{-1}\boldsymbol{U}\left(\boldsymbol{B}^{-1} + \boldsymbol{U}^\intercal\boldsymbol{A}^{-1}\boldsymbol{U}\right)^{-1}\boldsymbol{U}^\intercal\boldsymbol{A}^{-1}.$$

B Proof of Theorem 3.4

The proof starts by establishing a random equivalent for the normalised Adjacency operator given by $\tilde{\boldsymbol{A}} = \frac{1}{\sqrt{n}}(\boldsymbol{A} - \boldsymbol{q}\boldsymbol{q}^\intercal)$. By Assumptions 2, 3 and 5, we have straightforwardly that, almost surely

$$\left\|\tilde{\boldsymbol{A}} - \left(q^2\eta\bar{\boldsymbol{y}}\bar{\boldsymbol{y}}^\intercal + \frac{1}{\sqrt{n}}\boldsymbol{N}\right)\right\| \to 0, \tag{14}$$

where $\boldsymbol{N}$ is a random matrix with i.i.d. entries of zero mean and variance $\nu = q^2(1-q^2)$. Besides, since $\mathbb{E}[\boldsymbol{X}\boldsymbol{X}^\intercal] = \frac{\|\boldsymbol{\mu}\|^2}{c}\bar{\boldsymbol{y}}\bar{\boldsymbol{y}}^\intercal + \boldsymbol{I}_n$, letting $\gamma_f = \|\boldsymbol{\mu}\|^2$ and $\gamma_g = q^2\eta$, we consider the equivalent multiplicative model for $\boldsymbol{Y}$ defined as

$$\boldsymbol{Y} = \left(\gamma_g\bar{\boldsymbol{y}}\bar{\boldsymbol{y}}^\intercal + \frac{1}{\sqrt{n}}\boldsymbol{N}\right)\left(\frac{\gamma_f}{c}\bar{\boldsymbol{y}}\bar{\boldsymbol{y}}^\intercal + \boldsymbol{I}_n\right)^{\frac{1}{2}}\boldsymbol{Z},$$

where $\boldsymbol{Z}$ is random matrix with i.i.d. entries of zero mean and variance $\frac{1}{p}$. Conditionally on $\boldsymbol{N}$, applying Theorem A.1 for $\boldsymbol{M} = \left(\gamma_g\bar{\boldsymbol{y}}\bar{\boldsymbol{y}}^\intercal + \frac{1}{\sqrt{n}}\boldsymbol{N}\right)\left(\frac{\gamma_f}{c}\bar{\boldsymbol{y}}\bar{\boldsymbol{y}}^\intercal + \boldsymbol{I}_n\right)^{\frac{1}{2}}$, a deterministic equivalent of $\boldsymbol{Q}_{\boldsymbol{Y}}(z) = (\boldsymbol{Y}\boldsymbol{Y}^\intercal + z\boldsymbol{I}_n)^{-1}$ is given by

$$\bar{\boldsymbol{Q}}_{\boldsymbol{Y}|\boldsymbol{N}}(z) = \left(\frac{\left(\gamma_g\bar{\boldsymbol{y}}\bar{\boldsymbol{y}}^\intercal + \frac{1}{\sqrt{n}}\boldsymbol{N}\right)\left(\frac{\gamma_f}{c}\bar{\boldsymbol{y}}\bar{\boldsymbol{y}}^\intercal + \boldsymbol{I}_n\right)\left(\gamma_g\bar{\boldsymbol{y}}\bar{\boldsymbol{y}}^\intercal + \frac{1}{\sqrt{n}}\boldsymbol{N}\right)}{1+\delta_1(z)} + z\boldsymbol{I}_n\right)^{-1} \tag{15}$$

$$= \left(\frac{\boldsymbol{U}\boldsymbol{B}\boldsymbol{U}^\intercal + \frac{1}{n}\boldsymbol{N}\boldsymbol{N}^\intercal}{1+\delta_1(z)} + z\boldsymbol{I}_n\right)^{-1} \tag{16}$$

where

$$\boldsymbol{U} = [\bar{\boldsymbol{y}}, \boldsymbol{\phi}] \in \mathbb{R}^{n\times 2}, \quad \boldsymbol{B} = \begin{bmatrix} \gamma_2^2\left(\frac{\gamma_1}{c}+1\right) & \left(\frac{\gamma_1}{c}+1\right)\gamma_2 \\ \left(\frac{\gamma_1}{c}+1\right)\gamma_2 & \frac{\gamma_1}{c} \end{bmatrix} \tag{17}$$

with $\boldsymbol{\phi} = \frac{1}{\sqrt{n}}\boldsymbol{N}\bar{\boldsymbol{y}}$, $\bar{\boldsymbol{y}} = \boldsymbol{y}/\sqrt{n}$ and $\delta_1(z) = \frac{1}{p}\operatorname{Tr}\left(\left(\boldsymbol{U}\boldsymbol{B}\boldsymbol{U}^\intercal + \frac{1}{n}\boldsymbol{N}\boldsymbol{N}^\intercal\right)\bar{\boldsymbol{Q}}_{\boldsymbol{Y}|\boldsymbol{N}}(z)\right)$. Applying Lemma A.2, $\delta_1(z)$ is simply the solution to $\delta_1(z) = \frac{1}{p}\operatorname{Tr}\left(\frac{1}{n}\boldsymbol{N}\boldsymbol{N}^\intercal\bar{\boldsymbol{Q}}_{\boldsymbol{Y}|\boldsymbol{N}}(z)\right)$. Moreover, defining the matrix $\bar{\boldsymbol{Q}}^{-\boldsymbol{B}}_{\boldsymbol{Y}|\boldsymbol{N}}(z) = \left(\frac{\frac{1}{n}\boldsymbol{N}\boldsymbol{N}^\intercal}{1+\delta_1(z)} + z\boldsymbol{I}_n\right)^{-1}$, we have by Lemma A.3

$$\bar{\boldsymbol{Q}}_{\boldsymbol{Y}|\boldsymbol{N}}(z) = \bar{\boldsymbol{Q}}^{-\boldsymbol{B}}_{\boldsymbol{Y}|\boldsymbol{N}}(z) - \bar{\boldsymbol{Q}}^{-\boldsymbol{B}}_{\boldsymbol{Y}|\boldsymbol{N}}(z)\boldsymbol{U}\left((1+\delta_1(z))\boldsymbol{B}^{-1} + \boldsymbol{U}^\intercal\bar{\boldsymbol{Q}}^{-\boldsymbol{B}}_{\boldsymbol{Y}|\boldsymbol{N}}(z)\boldsymbol{U}\right)^{-1}\boldsymbol{U}^\intercal\bar{\boldsymbol{Q}}^{-\boldsymbol{B}}_{\boldsymbol{Y}|\boldsymbol{N}}(z). \tag{18}$$

Again by Theorem A.1, a deterministic equivalent of $\bar{\boldsymbol{Q}}^{-\boldsymbol{B}}_{\boldsymbol{Y}|\boldsymbol{N}}(z)$ is given by

$$\bar{\boldsymbol{Q}}^{-\boldsymbol{B}}_{\boldsymbol{Y}}(z) = \left(\frac{\nu\boldsymbol{I}_n}{(1+\delta_1(z))(1+\delta_2(z))} + z\boldsymbol{I}_n\right)^{-1} = \frac{(1+\delta_1(z))(1+\delta_2(z))}{\nu + z(1+\delta_1(z))(1+\delta_2(z))}\boldsymbol{I}_n \tag{19}$$

where $\delta_2(z)$ is the unique solution to $\delta_2(z) = \frac{1}{n}\operatorname{Tr}\left(\frac{\nu\boldsymbol{I}_n}{(1+\delta_1(z))}\bar{\boldsymbol{Q}}^{-\boldsymbol{B}}_{\boldsymbol{Y}}(z)\right) = \frac{\nu(1+\delta_2(z))}{\nu+z(1+\delta_1(z))(1+\delta_2(z))}$, and similarly $\delta_1(z)$ satisfies $\delta_1(z) = \frac{1}{c}\frac{\nu(1+\delta_1(z))}{\nu+z(1+\delta_1(z))(1+\delta_2(z))}$. Therefore, replacing $\bar{\boldsymbol{Q}}^{-\boldsymbol{B}}_{\boldsymbol{Y}|\boldsymbol{N}}(z)$ in (18) by its deterministic equivalent $\bar{\boldsymbol{Q}}^{-\boldsymbol{B}}_{\boldsymbol{Y}}(z)$ and since $\boldsymbol{U}^\intercal\boldsymbol{U} \to \boldsymbol{T}$ almost surely, provides the final result of Theorem 3.4.

Table 1: Statistics of the datasets used in our experiments.

DATASET	#FEATURES	#NODES	#EDGES	#CLASSES
CORA	1433	2708	5208	7
CITESEER	3703	3327	4552	6
PUBMED	500	19717	44338	3
CORA-FULL	8710	18703	62421	67
COMPUTERS	767	13381	245778	10
PHOTO	745	7487	119043	8

C Proof of Corollary 3.5

Following the same procedure as in Section B, when $\eta = 0$, a deterministic equivalent for $\boldsymbol{Q}_{\boldsymbol{Y}}(z)$ takes the form

$$\bar{\boldsymbol{Q}}_{\boldsymbol{Y}}(z) = \zeta(z)(1+\delta_1(z))\left(\boldsymbol{I}_n - \frac{\zeta^2(z)\gamma_f}{c+\nu\gamma_f\zeta(z)}\boldsymbol{\phi}\boldsymbol{\phi}^\intercal\right). \tag{20}$$

By definition of the deterministic equivalent, we have almost surely

$$|\bar{\boldsymbol{y}}^\intercal\hat{\boldsymbol{y}}|^2 = \frac{-1}{2\pi i}\oint_\Gamma \bar{\boldsymbol{y}}^\intercal\boldsymbol{Q}_{\boldsymbol{Y}}(-z)\bar{\boldsymbol{y}}dz \to_{n\to\infty} \frac{-1}{2\pi i}\oint_\Gamma \bar{\boldsymbol{y}}^\intercal\bar{\boldsymbol{Q}}_{\boldsymbol{Y}}(-z)\bar{\boldsymbol{y}}dz. \tag{21}$$

Hence, we need to evaluate the Cauchy-integral $\frac{-1}{2\pi i}\oint_\Gamma \bar{\boldsymbol{y}}^\intercal\bar{\boldsymbol{Q}}_{\boldsymbol{Y}}(-z)\bar{\boldsymbol{y}}dz$. In particular, the quadratic form $\bar{\boldsymbol{y}}^\intercal\bar{\boldsymbol{Q}}_{\boldsymbol{Y}}(z)\bar{\boldsymbol{y}}$ evaluates as

$$\bar{\boldsymbol{y}}^\intercal\bar{\boldsymbol{Q}}_{\boldsymbol{Y}}(z)\bar{\boldsymbol{y}} = \zeta(z)(1+\delta_1(z))\left(1 - \frac{\zeta^2(z)\gamma_f}{c+\nu\gamma_f\zeta(z)}\bar{\boldsymbol{y}}^\intercal\boldsymbol{\phi}\boldsymbol{\phi}^\intercal\bar{\boldsymbol{y}}\right) \to_{n\to\infty} \zeta(z)(1+\delta_1(z)).$$

Indeed, since the mapping $\boldsymbol{X} \mapsto \frac{1}{\sqrt{n}}\bar{\boldsymbol{y}}^\intercal\boldsymbol{X}\bar{\boldsymbol{y}}$ is $\frac{1}{\sqrt{n}}$-Lipschitz transformation w.r.t. the Frobenius norm $\|\cdot\|_F$, then we have the concentration inequality, for all $t \geq 0$

$$\mathbb{P}\left(\left|\frac{1}{\sqrt{n}}\bar{\boldsymbol{y}}^\intercal\boldsymbol{N}\bar{\boldsymbol{y}} - \mathbb{E}\left[\frac{1}{\sqrt{n}}\bar{\boldsymbol{y}}^\intercal\boldsymbol{N}\bar{\boldsymbol{y}}\right]\right| > t\right) \leq C\, e^{-(\sqrt{n}\,t/\nu)^2}, \tag{22}$$

for some constant $C \geq 0$ independent of n. In particular, since $\mathbb{E}\left[\frac{1}{\sqrt{n}}\bar{\boldsymbol{y}}^\intercal\boldsymbol{N}\bar{\boldsymbol{y}}\right] = 0$, we have

$$\mathbb{P}\left(\left|\left(\frac{1}{\sqrt{n}}\bar{\boldsymbol{y}}^\intercal\boldsymbol{N}\bar{\boldsymbol{y}}\right)^2 - \mathbb{E}\left[\left(\frac{1}{\sqrt{n}}\bar{\boldsymbol{y}}^\intercal\boldsymbol{N}\bar{\boldsymbol{y}}\right)^2\right]\right| > t\right) \leq C\, e^{-\frac{\sqrt{n}\,t}{2\nu}}, \tag{23}$$

which shows that $\bar{\boldsymbol{y}}^\intercal\boldsymbol{\phi}\boldsymbol{\phi}^\intercal\bar{\boldsymbol{y}} = \left(\frac{1}{\sqrt{n}}\bar{\boldsymbol{y}}^\intercal\boldsymbol{N}\bar{\boldsymbol{y}}\right)^2$ concentrates around its mean value, with

$$\mathbb{E}\left[\left(\frac{1}{\sqrt{n}}\bar{\boldsymbol{y}}^\intercal\boldsymbol{N}\bar{\boldsymbol{y}}\right)^2\right] = \frac{1}{n}\mathrm{Var}\left[\bar{\boldsymbol{y}}^\intercal\boldsymbol{N}\bar{\boldsymbol{y}}\right] = \frac{1}{n}\sum_{i,j=1}^n \bar{y}_i^2\bar{y}_j^2\mathrm{Var}[N_{ij}] = \frac{\|\bar{\boldsymbol{y}}\|^4\,\nu}{n} \to 0.$$

Therefore, $\bar{\boldsymbol{y}}^\intercal\boldsymbol{\phi}\boldsymbol{\phi}^\intercal\bar{\boldsymbol{y}} \to 0$ almost surely as $n \to \infty$. The final step consists in evaluating the integral $\frac{1}{2\pi i}\oint_\Gamma \zeta(-z)(1+\delta_1(-z))dz = 0$ since the function $z \mapsto \zeta(-z)(1+\delta_1(-z))$ does not have singularities on the contour Γ. Indeed, this integral corresponds to the only noise case from the data model (i.e., $\boldsymbol{Y} = \frac{1}{\sqrt{n}}\boldsymbol{N}\boldsymbol{Z}$).

D Datasets and Implementation Details

Statistics of the datasets we used are summarised in Table 1. As mentioned in the main paper, we experiment on citation networks of Cora/CiteSeer/Pubmed/CoraFull (Sen et al. 2008, Shchur et al. 2018), as well as Amazon co-purchase networks of Photo/Computers (Shchur et al. 2018). For train/valid/test splits, we follow the public split on Cora/CiteSeer/PubMed and construct the train/valid/test set on CoraFull/Photo/Computers by randomly sampling 20 nodes from each class to

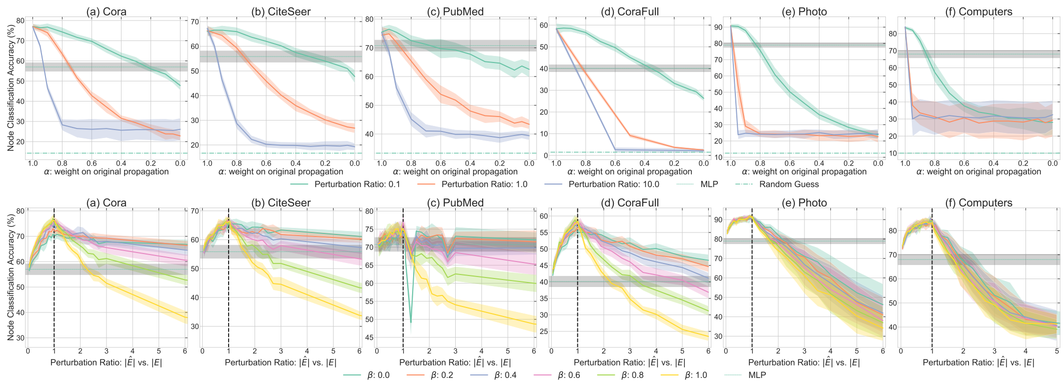

Figure 4: Results of Experiments averaged over multiple train/valid/test splits. **(top row)** Theoretical Noise Scheme: Performance change over the coefficient of original graph propagation, α, with different perturbation ratios. **(bottom row)** Realistic Noise Scheme: Performance change over the perturbation ratio under realistic setting with different coefficients, β, put on the noisy graph propagation.

form the training set and 500/1000 nodes respectively from the rest to form the validation and test set, as proposed in Yang et al. (2016).

In line with our theoretical analysis, the main GCN architecture on which we experimented in this paper is a single-layer GCN (one iteration of message passing and update) stacked with a Multi-Layer Perception (MLP). The objective of the experiments is to validate our theoretical hypotheses and experiment with the robustness of GCN models under graph structure perturbation. We also study empirically to what extent the validated hypotheses extrapolate to scenarios where deeper GCN architectures with multiple layers of graph propagation are used and/or node features are also perturbed.

All the experiments are performed with the Adam optimiser (Kingma & Ba 2014) and the same set of hyper-parameters, with learning rate being 1e-2, number of epochs being 200 and feature hidden dimension being 128. We repeat each experiment 10 times and report the resulting means and standard deviations to eliminate the impact of random initialisation.

We have made our implementation publicly available online[9]. It is built upon the open source library *PyTorch Geometric* (PyG) under MIT license (Fey & Lenssen 2019). The experiments are run on a Intel(R) Xeon(R) W-2123 processor with 64GB ram and a NVIDIA GeForce RTX 2080Ti GPU with 12GB ram.

E Multiple Splits

Shchur et al. (2018) argue that different train/valid/test splits of datasets may have a non-negligible impact on the performance of GNN models for the node classification task. To investigate the influence of different splits on our hypothesis, we construct train/valid/test split for each dataset following Yang et al. (2016) over 10 random seeds. As each experiment is repeated 10 times, a total of 100 results is obtained for a specific setting, i.e., specific α or β or γ and noise ratio. Similar to the results of one split, we report the mean and standard deviations of the 100 results in Figure 4. Although the standard deviation increases since we introduce more variation in the multi-split setting, the general trend remains the same, as shown in Figure 4. Our conclusion drawn in the main text still holds: *perturbations of the graph structure strongly influence the performance of the GCN and adding a node feature kernel can robustify the GCN against such perturbations.*

F Multi-layer GCN

In this set of experiments, we observe to what extent the conclusions drawn in our theoretical analysis carry over to deeper GCN architectures. We add an extra message passing layer to the previous

[9] `https://github.com/ChangminWu/RobustGCN`

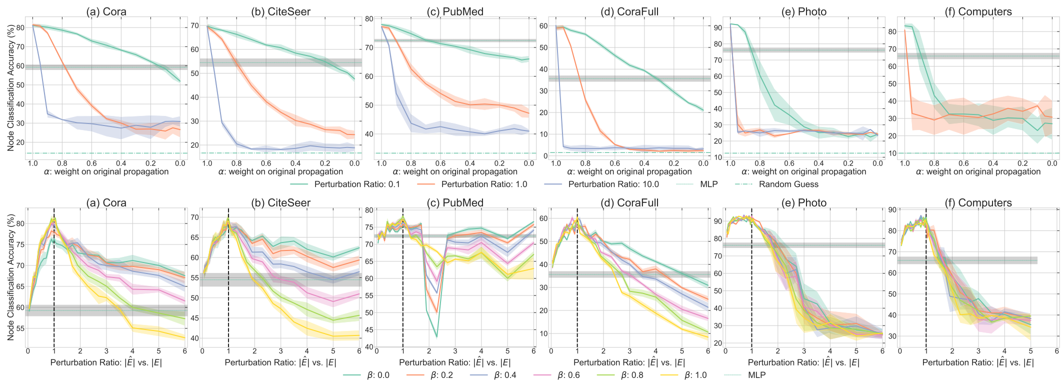

Figure 5: Results of multi-player GCN model. **(top row)** Theoretical Noise Scheme: Performance change over the coefficient of original graph propagation, α, with different perturbation ratios. Notice that on (f) for Computers, the results of perturbation ratio equals 10 is missing as the computation is out of GPU memory. **(bottom row)** Realistic Noise Scheme: Performance change over the perturbation ratio under realistic setting with different coefficients, β, put on the noisy graph propagation.

single-layer model and repeat our experiments on this deeper model. Part of the results have already been shown in Section 4.1 of the main paper. In Figure 5 we show the full set of results for all six datasets and are able to confirm the trends observed for the single-layer model.